Chapter 3

Cavitation Wear of Structural Ceramics

Zbigniew Pędzich

Additional information is available at the end of the chapter

http://dx.doi.org/10.5772/intechopen.79510

Abstract

The usage of advanced ceramic materials in the applications endangered by intensive cavitation could limit erosion phenomena distinctly. In the presented work, cavitation erosion resistance of ceramics the most commonly used in structural applications was investigated. These materials were oxide ones: α-alumina, yttria-stabilized tetragonal zirconia, and two composites selected from alumina/zirconia system. Otherwise, the most promising non-oxide materials were examined: silicon carbide and silicon nitride. Results showed significant difference in cavitation wear mechanisms of all investigated materials. Degradation of alumina proceeded from the beginning on the relatively large surfaces, and the dominant mechanism of destruction was removing of the whole grains. Degradation of zirconia also consisted on removing of the whole grains, but this process proceeded locally, along ribbon-like paths. Cavitation wear of composites was strongly influenced by the residual stresses caused by the thermal expansion coefficient mismatch. Cavitation erosion of silicon nitride proceeded by selective degradation of glassy phase present on grain boundaries. On the contrary, silicon carbide degradation proceeded by large grain fragmentation process.

Keywords: cavitation wear, alumina, zirconia, silicon carbide, silicon nitride, composites

1. Introduction

Phenomenon of cavitation could be described as reproducible process of nucleation, growth, and violent collapse of clouds of bubbles within the liquid. As a consequence of implosion of cavitation bubbles, microstreams of liquid are produced, and pressure waves assisting bubble disappearing process become the main reason of material damage. This damage consists in a material loss called cavitation erosion. Mentioned process starts on material surface

and depending on material properties develops locally on bigger surface areas or proceeds into material bulk. The nature of loading caused by the interaction between pressure waves, microstream blows, and intensive hydrodynamics parameters is presented by many researchers as fatigue process [1–3]. As a result of such approach, improvement of cavitation resistance of materials should be reached by the material hardness and micro-hardness increase, the mean grain size decrease, and introduction of internal compressive stresses (in the case of multiphase materials) [4–6]. Progress in cavitation resistance in metallic materials was reached by using intermetallic phases [7, 8]. Modern demands for reliability of fluid-flow machinery components forced application of ceramic phases as possible more resistant for cavitation damage than any metallic phase. Investigations of cavitation erosion of ceramics are not very often. Sparse reports [9–18] concern such materials like monophase oxides (α-alumina, tetragonal zirconia), silicon nitride, or some types of glassy phases. The mentioned works gave, as a result, some experimental data which put in order cavitation wear resistance of ceramic phases, suggesting explanations how the microstructure of sintered bodies could influence their susceptibility to cavitation wear. The presented work summarizing results of investigations of cavitation erosion resistance of commonly used, in structural applications, oxide (α-alumina and tetragonal zirconia, composites in alumina/zirconia system) and non-oxide (silicon carbide, silicon nitride) subjected to intensive, long-lasting (6000 min) jet-impact tests was investigated.

2. Experimental

The process of cavitation wear was investigated for six ceramic materials. Four of them were the widely used oxide materials: α-alumina, tetragonal zirconia, and two composites in alumina/zirconia system. The first one was an alumina-based material containing 10 vol.% of zirconia additive and the second one was zirconia based with 10 vol.% of alumina particles. For fabrication of sintered bodies, commercial powders were utilized: Al_2O_3—TM-DAR produced by Taimicron Inc., Japan (the mean crystallite size of 130 nm), and yttria-stabilized ZrO_2 powder named 3Y-TZ manufactured by Tosoh, Japan (the mean crystallite size of 20 nm). Composite powders were manufactured by rotation-vibration mixing of constituent powders. The mixing procedure was conducted in ethyl alcohol suspension for 1 h. After separation from milling media (5 mm zirconia balls), composited powders were dried and granulated. Preliminary compaction of powders was performed uniaxially in ceramic die under pressure of 50 MPa. After that, samples were isostatically repressed under 300 MPa. Pressureless sintering process was conducted at 1500 (for alumina) or 1550°C (for the rest of oxide materials). The dwelling time of 2 h was the same for all the mentioned samples. Mentioned procedure allowed to achieve samples which have cylindrical shape of 20 mm in diameter and 6 ± 0.5 mm high. Description of oxide materials investigated in this work was as follows: **A**, **Z**, **AZ**, and **ZA** for alumina, zirconia, alumina/zirconia composite, and zirconia/alumina composite, respectively.

Silicon carbide (**SC**) samples were prepared utilizing commercial powder (SIKA FCP 15, Saint-Gobain). Compaction conditions were identical as for oxide materials. Sintering procedure was as follows: heating 10°C/min up to 1800°C, 5°C/min in the range of 1800–2150°C. Dwelling time at 2150°C was 1 h and the sintering atmosphere was argon.

Silicon nitride (**SN**) material was prepared on the base of Si_3N_4 H.C. STARCK powder and oxide additives in 4 wt.% Y_2O_3 (POCh, Lublin, Poland) and 6 wt.% of Al_2O_3 TM-DAR. The final powder was prepared by rotation-vibration wet mixing of constituent powders for 1 h in the environment of isopropyl alcohol. Composite powders after separation from milling media (5 mm silicon nitride balls) were dried and granulated. Compaction conditions were identical as for previously described materials. Sintering process was carried on at 1800°C for 2 h in nitrogen atmosphere.

Densification (relative density ρ) of each material was calculated as a reference of apparent density measured by Archimedes method (at 21°C) to the theoretical values ($d_{ZrO2} = 6.10$ g/cm^3, $d_{SiC} = 3.21$ g/cm^3, $d_{Si3N4} = 3.21$ g/cm^3, $d_{Al2O3} = 3.99$ g/cm^3, $d_{Y2O3} = 5.01$ g/cm^3). Relative density for silicon carbide samples was calculated considering the content of phases arising due to oxide addition. Densification of materials (as relative density values) was collected in **Table 1**.

Basic mechanical properties were determined as follows: hardness (*HV*) and fracture toughness (K_{Ic}) were investigated by the Vickers indentation method. The values of K_{Ic} parameter were calculated basing on the Niihara model [19]. Data for calculations were collected utilizing Nanotech MV-700 equipment. The load was 49.05 N for hardness and 98.1 N for K_{Ic} measurements. The data for bending strength (σ) analysis were delivered by the four-point bending tests performed on 45 mm × 4 mm × 3 mm bars (Zwick Roell testing machine). The ultrasonic method was used for Young's moduli of sintered body determination.

Cavitation erosion process was examined utilizing jet-impact device, described in detail in [7]. The sample surface roughness, measured before the test (PGM-1 C profilometer), was less than 0.03 μm for all samples. Cavitation wear test consists in fast rotation of samples which stroke against the water stream. The samples were mounted vertically in rotor arms, parallel to the axis of water stream. Water was pumped continuously at 0.06 MPa through a nozzle with a 10 mm diameter, 1.6 mm away from the sample edge. Water flow intensity was constant and amounted to 1.55 m^3/h. The wear rate was determined by sample weighing up to the total time of 6000 min. The wear rate was determined after each 600 min of the test as the weight loss of each sample. The samples were dried before weighing in a laboratory dryer at 120°C for 60 min. The volumetric wear rates were calculated using apparent density of each sample type and their weight loss. Surfaces of the worn materials were examined by means of the SEM technique using FEI Nova Nano 200 device.

Material	Relative density, ρ, % of theo. ±0.02	Vickers hardness, *HV*, GPa	Young modulus, *E*, GPA	Fracture toughness, K_{Ic}, MPam$^{0.5}$	Bending strength, σ, MPa
Al_2O_3—**A**	99.28	17.0 ± 1.2	379 ± 6	4.3 ± 0.2	600 ± 120
ZrO_2—**Z**	99.96	14.0 ± 0.5	209 ± 5	6.1 ± 0.3	1150 ± 55
Al_2O_3/ZrO_2—**AZ**	98.50	17.0 ± 0.4	361 ± 5	5.1 ± 0.5	800 ± 120
ZrO_2/Al_2O_3—**ZA**	99.12	15.0 ± 0.6	216 ± 4	6.0 ± 0.4	1050 ± 55
SiC—**SC**	98.50	27.2 ± 0.8	392 ± 6	6.3 ± 2.0	550 ± 100
Si_3N_4—**SN**	98.66	16.5 ± 0.9	301 ± 8	5.3 ± 1.1	720 ± 150

Table 1. Properties of investigated materials.

3. Results and discussion

Table 1 collects data concerning basic properties of investigated materials. The level of densification is described as relative density value. All investigated materials were dense, and the level of total porosity did not exceed 1.5% in any case. Basic mechanical properties, hardness, modulus of elasticity, bending strength, and fracture toughness were on the level which is typically reported for similar materials.

The basic results of the stream-impact test of oxide ceramics were collected in **Figure 1**. It presented the volumetric wear of the investigated samples. As it was predicted, ceramic phases were resistant to cavitation wear, yet the difference between alumina **A** and zirconia **Z** was distinct. The most interesting fact resulting from the wear investigations was that both composites **AZ** and **ZA** had much better cavitation resistance than zirconia.

Microstructural observations of eroded surfaces performed by means of SEM technique allowed to recognize differences in destruction mechanisms for investigated materials. Relatively high rate of erosion measured for alumina material could be explained by mechanism which could be distinctly recognized after eroded surface examination revealed in micrographs (**Figure 2**).

Destruction of alumina material happened by removing of whole grains. This process accelerated during the test duration and after 2400–3000 min was very intensive. Process of grain fragmentation was not observed. Transgranular cracking was detected in very rare number of cases (like a large grain in the center in **Figure 2** micrograph at the bottom). Seeing that, alumina grains were relatively large; degradation process after long exposition on cavitation was very significant.

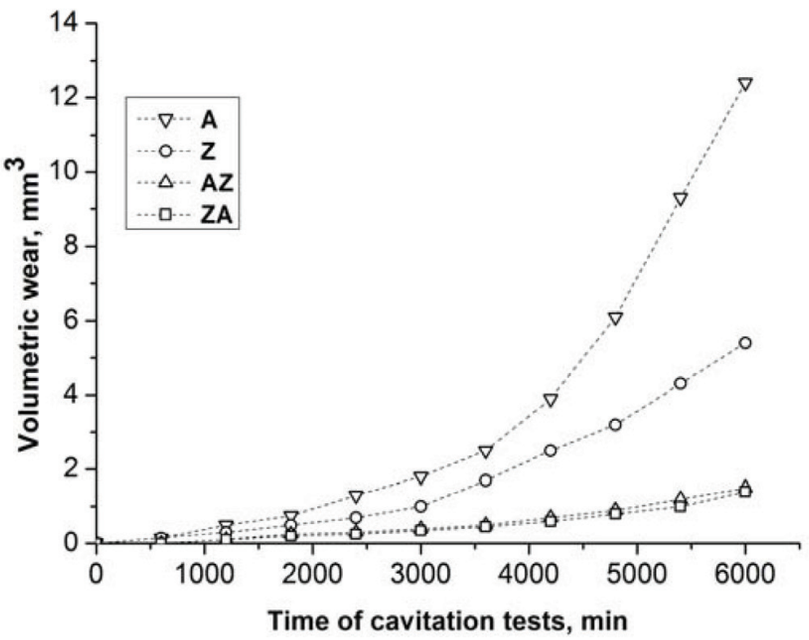

Figure 1. Results of volumetric loss measurements during stream-impact cavitation test of investigated oxide materials.

http://dx.doi.org/10.5772/intechopen.79510

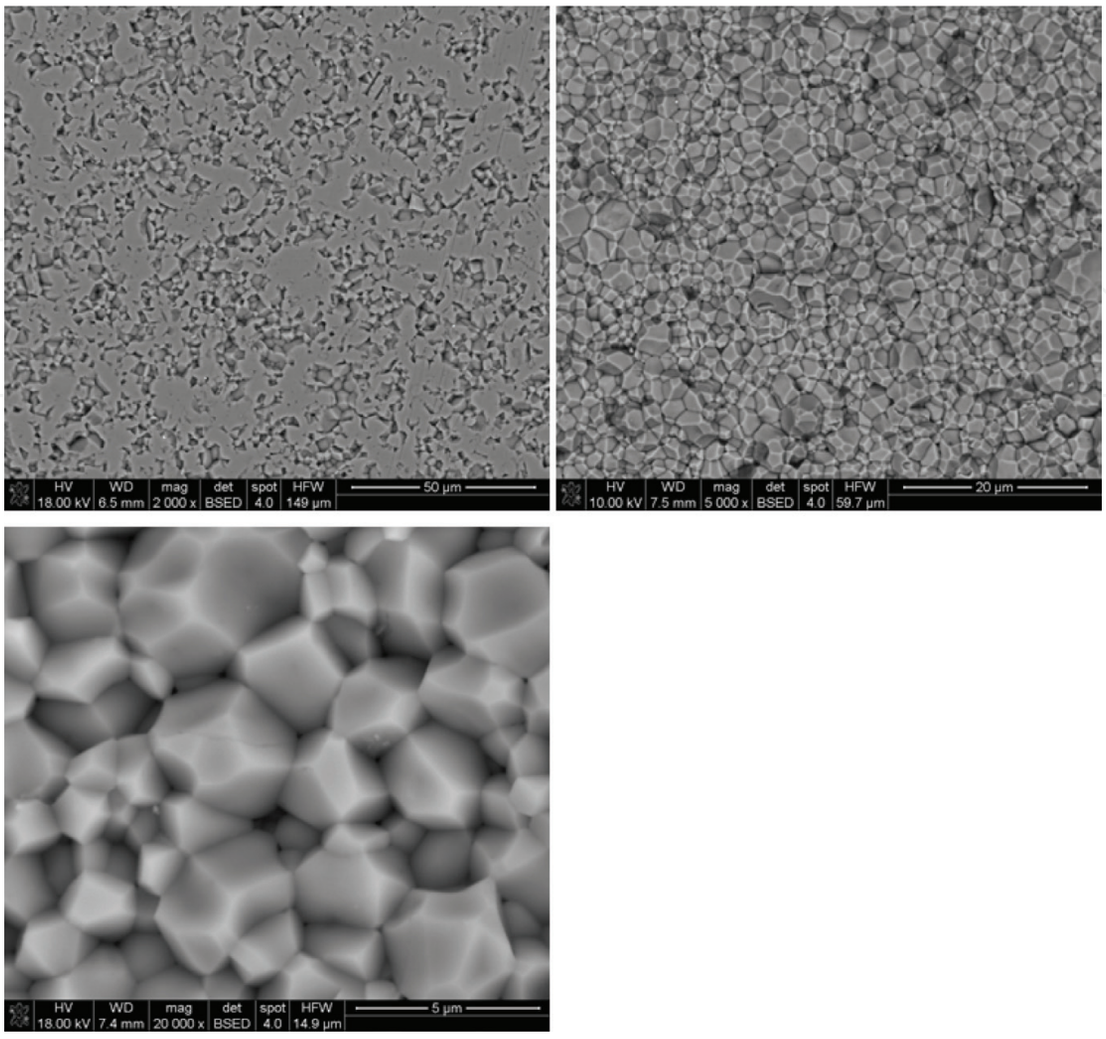

Figure 2. SEM microstructures of alumina material (**A**) on different stages of destruction—starting degradation of polished surface (after 600 min) (at the top left side) and advanced level of degradation (after 2400 min) (at the top right side and at the bottom).

Erosion process in zirconia materials runs in different ways. Microstructural documentation of this process was presented in **Figure 3**. Individual zirconia grains were removed from the surface, and this act consequently induced microcracks in this region [12]. Such situation made more probable possibility of removing the next grain in the nearest neighborhood created whole. This process runs not parallel to the sample surface but perpendicularly to it. This was the reason why erosion in zirconia developed in relatively limited surface area, and consequently the removed volume of the material is limited.

The way of degradation of composites depends on the major phase content. In **Figure 4**, selected areas of **AZ** composite microstructures were presented. When dispersion of constituent phases in composite was very good (on single micrometer level), surface was degraded uniformly. The mechanism of degradation was similar like in pure alumina material (whole grains removing), but in **AZ** composite, grains were much smaller than in pure alumina due to restraining influence of inert particles of minor phase (see Zener effect [20]). Additionally,

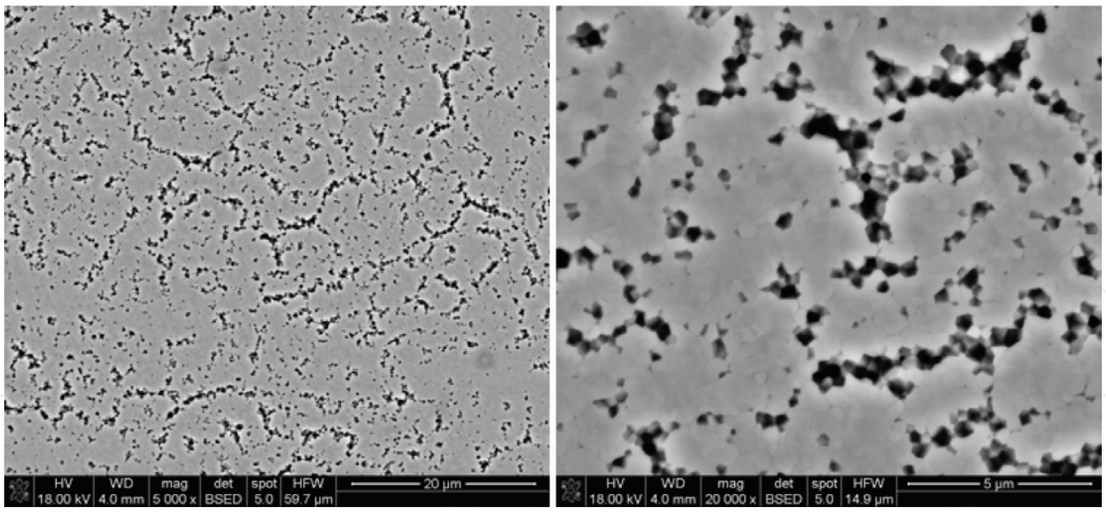

Figure 3. SEM microstructures of zirconia material (**Z**) on medium advanced level of destruction (after 2400 min), smaller magnification showing "paths" of removed grains (left side) and bigger magnification showing local depth of mentioned "paths"(right side).

residual stress state caused by coefficients of thermal expansion mismatch ($\alpha_{Al2O3} = 9.2 \cdot 10^{-6} °C^{-1}$; $\alpha_{ZrO2} = 11.0 \cdot 10^{-6} °C^{-1}$) [21] kept alumina matrix in average compressive stress state. As an effect of both mentioned factors acting, one can observe significantly limited cavitation erosion rate for **AZ** composite.

Detailed microstructural investigations showed that if some microstructural flaws were present in the composite (**Figure 4** right side) and homogeneity of its microstructure was not perfect (on the level of a few microns), large alumina agglomerates behave like pure alumina phase. Degradation of such agglomerates was faster than areas with well-dispersed zirconia grains, and the mechanism of degradation was identical than that observed for pure alumina (**A**).

Evidences of erosion in **ZA** composite presented in **Figure 5** proved that the main mechanism of material destruction was similar to that noticed for **Z** material. The **ZA** surfaces were covered by a net of erosion paths penetrating into material bulk. However, the surface density of mentioned paths is lower than that for **Z** material. Even if in some cases eroded areas reached diameters of a few microns (**Figure 5**, right side), a total erosion effect was smaller than that measured for pure zirconia phase.

It is worth to notice that the total level of volume loss for **AZ** and **ZA** materials was very similar. Such effect was not obvious because erosion rates for **A** and **Z** were distinctly different. Probably the strongest influence for such result has an effect of inhibition alumina matrix grain growth process in **AZ** material. Although the residual stress state in **AZ** and **ZA** materials was different (in **AZ** matrix was under compression, in **ZA** matrix was under tension), the total erosion rates were practically identical. In all investigated oxide materials, an elementary erosion act was the removing of the whole grain. The process of transgranular cracking was detected in very limited numbers of individual cases. It suggests that the decisive factor for

http://dx.doi.org/10.5772/intechopen.79510

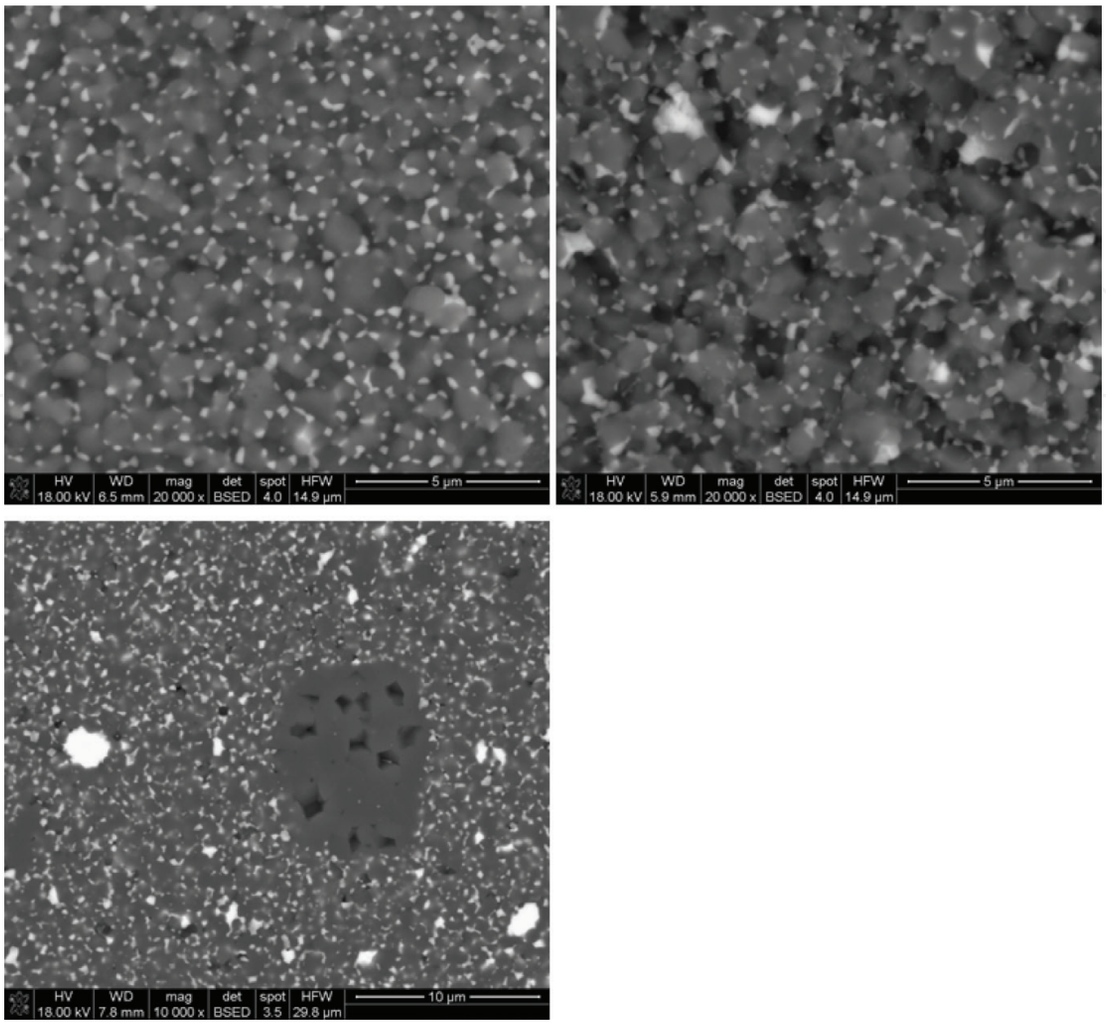

Figure 4. SEM microstructures of alumina/zirconia composite material (**AZ**): on medium advanced level of destruction, after 2400 min (at the top left side), and on strongly advanced level of destruction, after 5400 min (at the top right side), area with poor level of homogeneity (at the bottom). Light grains are zirconia ones; darker grains are alumina phase.

the erosion rate was the small grain size of materials. The direction of residual stresses played a not so important role. It is also important to underline that degradation of all investigated oxide materials went not linearly, but wear rate accelerated with the test duration.

Figure 6 presented volumetric losses of **A** and **Z** compared to non-oxide materials: silicon nitride (**SN**) and silicon carbide (**SC**). It is clearly visible that erosion rate for **SN** and **SC** was much smaller than that measured for oxide pure phases, but it is worth to notice that they were very close to values achieved for **AZ** and **ZA** composites.

Figure 7 illustrated the sequence of **SN** material degradation caused by cavitation. Microstructure of this material is composed of two elements—elongated silicon nitride grains (dark phase in micrographs) and oxynitride amorphous phase (light phase in micrographs) which was the liquid phase during sintering. The presence of liquid phase during sintering promoted very good densification of the material and helped to assure good mechanical properties. During

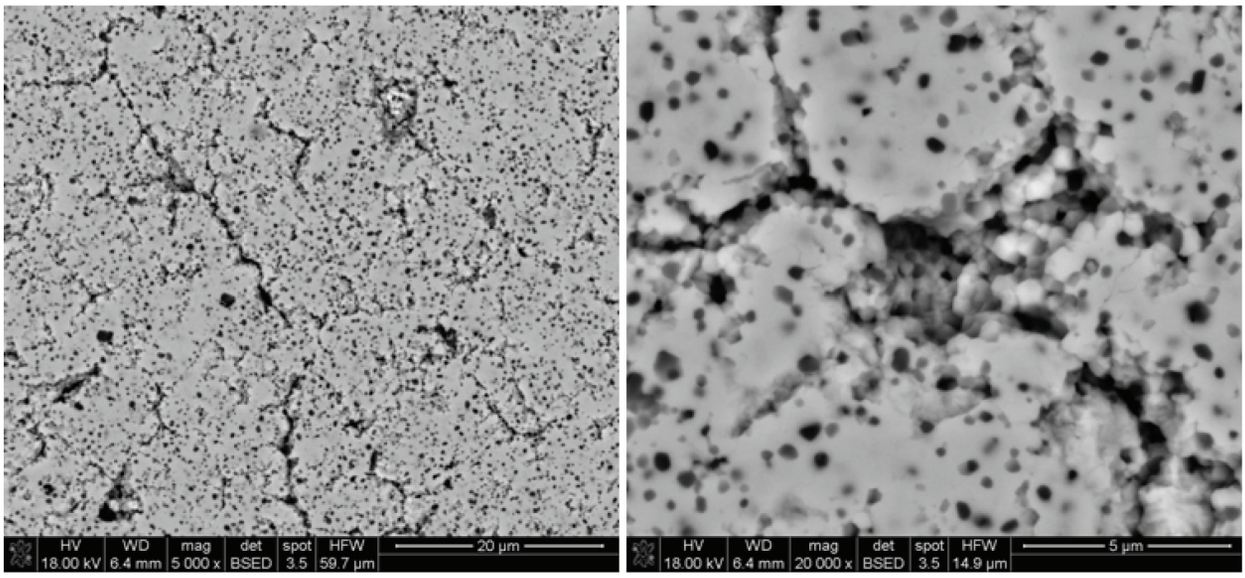

Figure 5. SEM microstructures of zirconia/alumina composite material (**ZA**) on relatively advanced level of destruction—area with very good constituent phase homogeneity (left side) and area with poor level of homogeneity (right side).

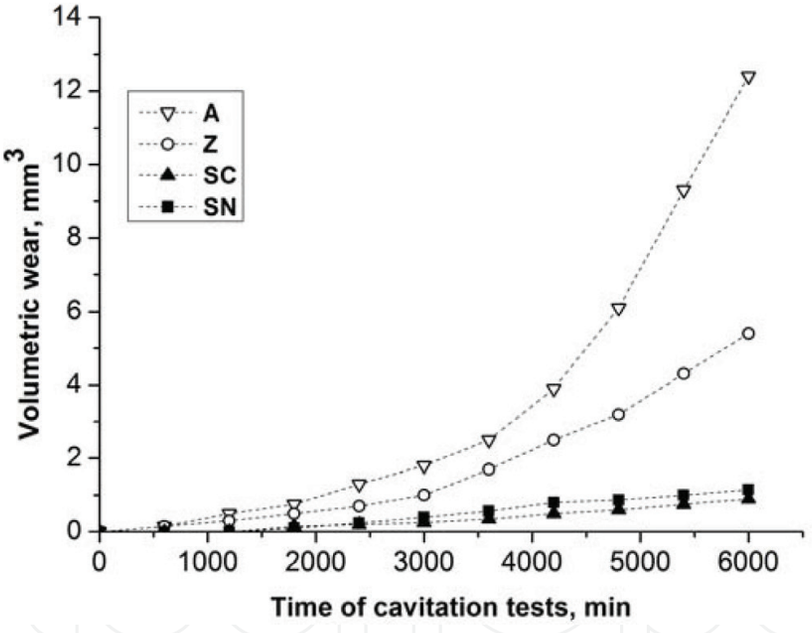

Figure 6. Results of volumetric losses during stream-impact cavitation test of alumina, zirconia, silicon carbide, and silicon nitride materials.

cavitation test, this phase seemed to be the weakest element of **SN** material microstructure. Erosion of **SN** started in oxynitride phase volume, and it proceeded through this phase. When this process was advanced enough, the whole silicon nitride grains could be removed. Probably, elongated shape of silicon carbide grains was profitable for erosion rate decrease. These elongated grains were trapped in bulk material, and they have not been removed so easily as it was observed for isometric oxide grains in previously mentioned materials (**A**, **Z**).

http://dx.doi.org/10.5772/intechopen.79510

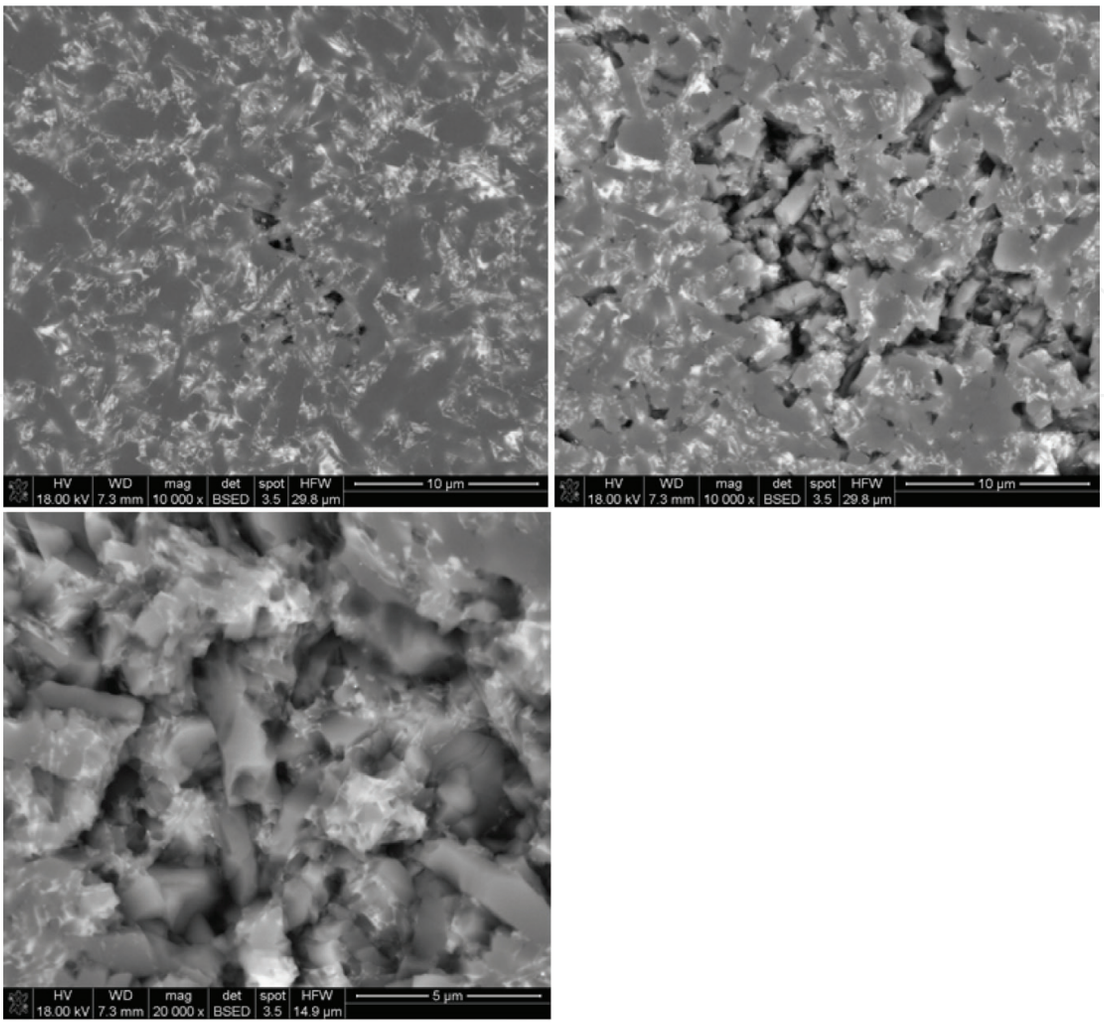

Figure 7. SEM microstructures of silicon nitride (**SN**) material at the first stages of destruction, 1800 min (at the top left side) and on more advanced levels of destruction, 3600 min (at the top right side) and 6000 min (at the bottom).

The most resistant for jet-impact cavitation test was silicon carbide material (**SC**). In **Figure 8** different stages of its degradation were presented. In this case mechanism of erosion was different from described previously. Volume of material loss proceeded in **SC** case not by the whole grains removing but by cracking of material (**Figure 8** left side) and removing of small parts of it (**Figure 8** right side). **Figure 9** illustrated development of mentioned process shoving a large part of eroded surface after different time of exposition for cavitation (3600 and 5400 min).

During jet-impact test procedure of data collecting consisted in measure of weight loss after every 600 min of test. In was not very dense net of experimental points due to rather high resistance of investigated materials for cavitation wear. Anyway, even not very frequent collection allowed to detect an important difference between oxide and non-oxide materials at the first stages of erosion. Measurable effect of material loss in oxide materials was detected from the beginning of the test. Measurements after 600 min showed distinct wear rate. For non-oxide

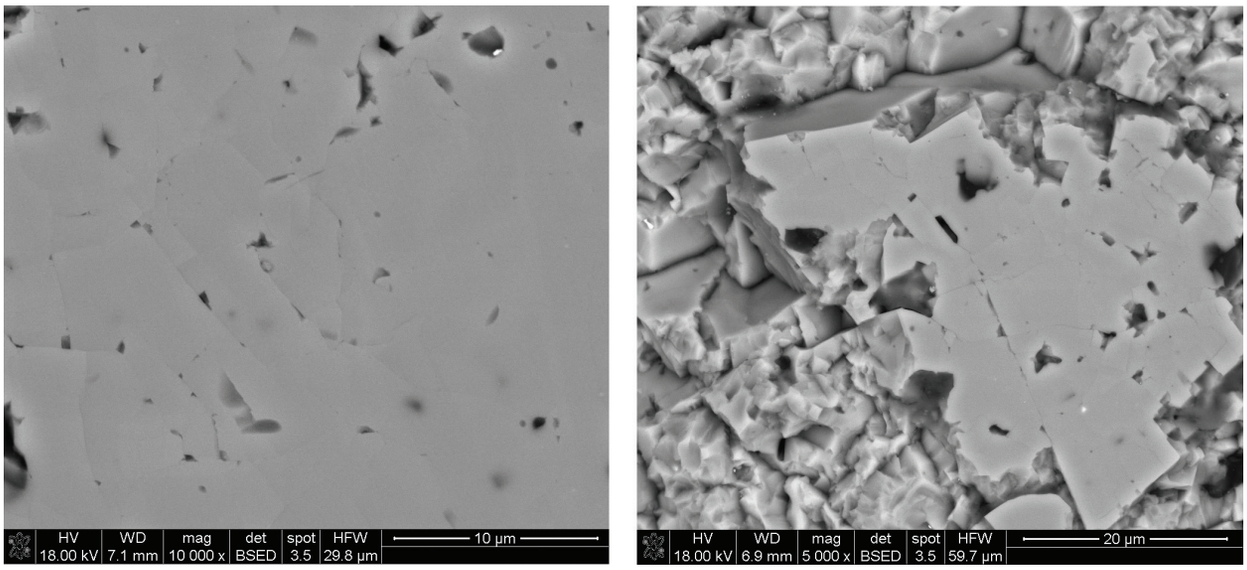

Figure 8. SEM microstructures of silicon carbide material (**SC**) at the first step of degradation, 1800 min (left side), and on relatively advanced level of destruction, 3600 min (right side).

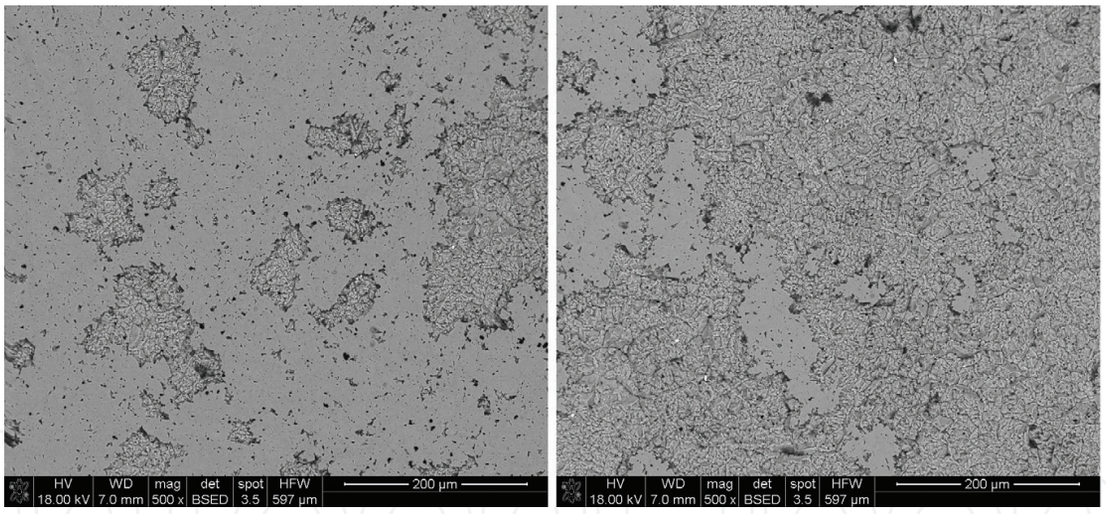

Figure 9. SEM microstructures of silicon carbide material (**SC**) after 3600 min (left side) and 5400 min (right side) duration of the jet-impact test.

materials (**SN** and **SC**), the first measurable effect of erosion was detected after 1800 min of test (**Figure 10**). This fact does not directly confirm that cavitation-caused erosion could be treated as an effect of a specific type of fatigue test. It confirms that different materials have a different threshold for degradation to start.

After the first period of stability, during the rest of performed cavitation test, the wear rates of **SC** and **SN** materials were practically stable contrary to systematical increment of wear rates for oxide materials (**Figure 6**).

http://dx.doi.org/10.5772/intechopen.79510

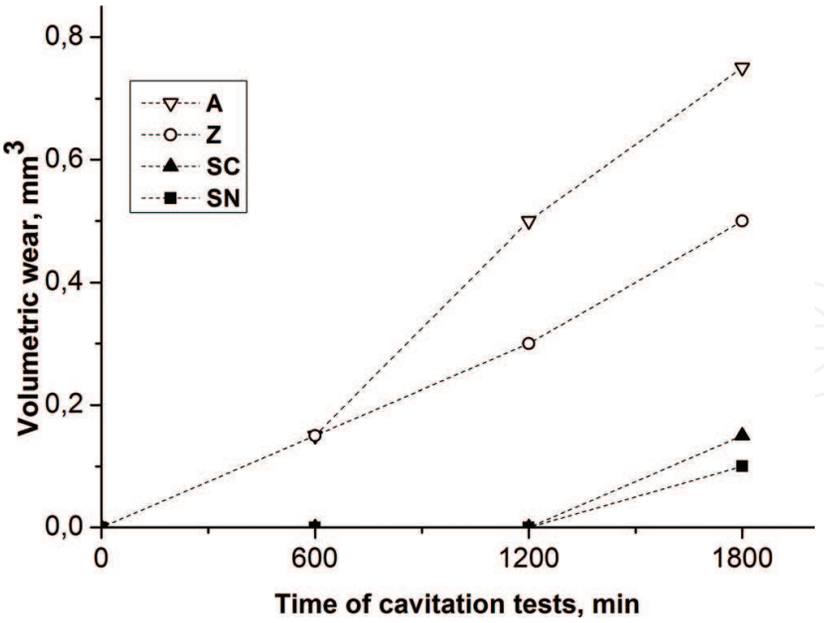

Figure 10. Results of volumetric losses during jet-impact cavitation test of alumina, zirconia, silicon carbide, and silicon nitride materials at the first stages of destruction.

4. Conclusions

Performed jet-impact cavitation test of a group of ceramic materials confirmed their relatively high resistance for cavitation erosion. Test revealed differences between mechanisms of degradation of materials subjected to cavitation and differences in measured wear rates.

Oxide materials degradation consisted in the whole grains removing from the bulk. Silicon nitride material eroded by faster degradation of amorphous phase which was the remnant of sintering process. Silicon carbide destruction is run by grain cracking and fragmentation.

Degradation of all oxide materials started relatively fast and proceeded in accelerated manner during the whole test. Contrary to that, non-oxide materials had a period of stability when any measurable mass losses were detected. After this period materials eroded in a stable manner, independently on test duration.

Composites in alumina/zirconia system have much better resistance for cavitation wear than alumina or zirconia monophase materials. This improvement could be described to profitable microstructural changes (finer grain size) and the presence of residual stresses which locally interact with stresses caused by cavitation.

Acknowledgements

Author would like to thank Dr. Magdalena Ziąbka from the Department of Ceramics and Refractory Materials of AGH University Krakow for very patient and competent assistance

during SEM observations and Dr. Robert Jasionowski from Maritime Academy Szczecin for its involvement in cavitation tests.

Author details

Zbigniew Pędzich

Address all correspondence to: pedzich@agh.edu.pl

Department of Ceramics and Refractory Materials, Faculty of Materials Science and Ceramics, AGH University of Science and Technology, Kraków, Poland

References

[1] Brennen CE. Cavitation and Bubble Dynamics. New York: Oxford University Press; 1995

[2] Briggs LJ. The limiting negative pressure of water. Journal of Applied Physics. 1970;**21**: 721-722

[3] Trevena DH. Cavitation and Tension in Liquids. Bristol: IOP Publishing Ltd; 1987

[4] Plesset MS, Chapman RB. Collapse of an initially spherical vapor cavity in the neighborhood of a solid boundary. Journal of Fluid Mechanics. 1971;**47**(2):283-290

[5] Hickling R, Plesset MS. Collapse and rebound of a spherical bubble in water. Physics of Fluids. 1964;**7**(1):7-14

[6] Naude CF, Ellis AT. On the mechanism of cavitation damage by non-hemispherical cavities collapsing in contact with a solid boundary. Journal of Basic Engineering. 1961;**83**: 648-656

[7] Jasionowski R, Przetakiewicz W, Zasada D. The effect of structure on the cavitational wear of FeAl intermetallic phase-based alloys with cubic lattice. Archives of Foundry Engineering. 2011;**11**(2):97-102

[8] Schneibel JH, George EP, Anderson IM. Tensile ductility, slow crack growth and fracture mode of ternary B2 iron aluminides at room temperature. Intermetallics. 1997;**5**:185-193

[9] Tomlinson WJ, Matthews SJ. Cavitation erosion of structural ceramics. Ceramics International. 1994;**20**(3):201-209

[10] Tomlinson WJ, Kalitsounakis N, Vekinis G. Cavitation erosion of aluminas. Ceramics International. 1999;**25**(4):331-338

[11] Niebuhr D. Cavitation erosion behavior of ceramics in aqueous solutions. Wear. 2007; **263**(1-6):295-300

[12] Garcia-Atance Fatjo G, Hadfield M, Tabeshfar K. Pseudoplastic deformation pits on polished ceramics due to cavitation erosion. Ceramics International. 2011;**37**:1919-1927

[13] Lua J, Zum Gahr K-H, Schneider J. Microstructural effects on the resistance to cavitation erosion of ZrO_2 ceramics in water. Wear. 2008;**265**:1680-1686

[14] Pedzich Z. The abrasive wear of alumina matrix particulate composites at different environments of work. In: Zhang D, Pickering K, Gabbitas B, Cao P, Langdon A, Torrens R, et al., editors. Advanced Materials and Processing IV. Vol. 29-30. Switzerland: Trans Tech Publications; 2007. pp. 283-286

[15] Pedzich Z. Fracture of oxide matrix composites with different phase arrangement. In: Dusza J, Danzer R, Morrell R, Quinn GD, editors. Fractography of Advanced Ceramics III: Key Engineering Materials. Vol. 409. Switzerland: Trans Tech Publications; 2009. pp. 244-251

[16] Pędzich Z, Jasionowski R, Ziąbka M. Cavitation wear of ceramics—Part I. Mechanisms of cavitation wear of alumina and tetragonal zirconia sintered polycrystals. Composites Theory and Practice. 2013;**13**(4):288-292

[17] Pędzich Z, Jasionowski R, Ziąbka M. Cavitation wear of ceramics—Part II. Mechanisms of cavitation wear of composites with oxide matrices. Composites Theory and Practice. 2014;**14**(3):139-144

[18] Pędzich Z, Jasionowski R, Ziąbka M. Cavitation wear of structural oxide ceramics and selected composite materials. Journal of the European Ceramic Society. 2014;**34**(14): 3351-3356. DOI: 10.1016/j.jeurceramsoc.2014.04.022

[19] Niihara K. A fracture mechanics analysis of indentation. Journal of Materials Science Letters. 1983;**2**:221-223

[20] Kang S-JL. Sintering: Densification, Grain Growth and Microstructure. Amsterdam: Elsevier; 2005

[21] Grabowski G, Pedzich Z. Residual stresses in particulate composites with alumina and zirconia matrices. Journal of the European Ceramic Society. 2007;**27**(2, 3):1287-1292

IntechOpen